

Supporting Information

Tracking high-valent surface iron species in the oxygen evolution reaction on cobalt iron (oxy)hydroxides

Seunghwa Lee,^a Aliko Moysiadou,^a You-Chiuan Chu,^b Hao Ming Chen,^b Xile Hu^{a,*}

^aLaboratory of Inorganic Synthesis and Catalysis, Institute of Chemical Sciences and Engineering, École Polytechnique Fédérale de Lausanne (EPFL), ISIC-LSCI, 1015 Lausanne, Switzerland

^bDepartment of Chemistry, National Taiwan University, Taipei 10617, Taiwan

* E-mail: xile.hu@epfl.ch

Table S1. Elemental compositions of Co and Fe determined by ICP-OES.

Elements			
Samples	Deposition time (sec)	Co (nmol)	Fe (nmol)
Fe 0%	40	4.45±0.1	
Fe 3.3%	45	4.2±0.12	0.14±0.15
Fe 7.2%	50	4.15±0.11	0.32±0.11
Fe 15%	55	3.82±0.1	0.65±0.13
Fe 23%	60	3.45±0.1	1.05±0.1
Fe 30%	70	3.1±0.08	1.35±0.11
Fe 42%	70	2.55±0.11	1.83±0.14

Table S2. Elemental compositions of Co and Fe of CoFeO_xH_y films at an Fe content of 30% as determined by ICP-OES.

Elements		
Deposition time (min)	Co (nmol)	Fe (nmol)
1	3.0	1.3
2	6.1	2.75
3	9.15	3.92
4.5	13.63	5.62
6	18.42	8.12

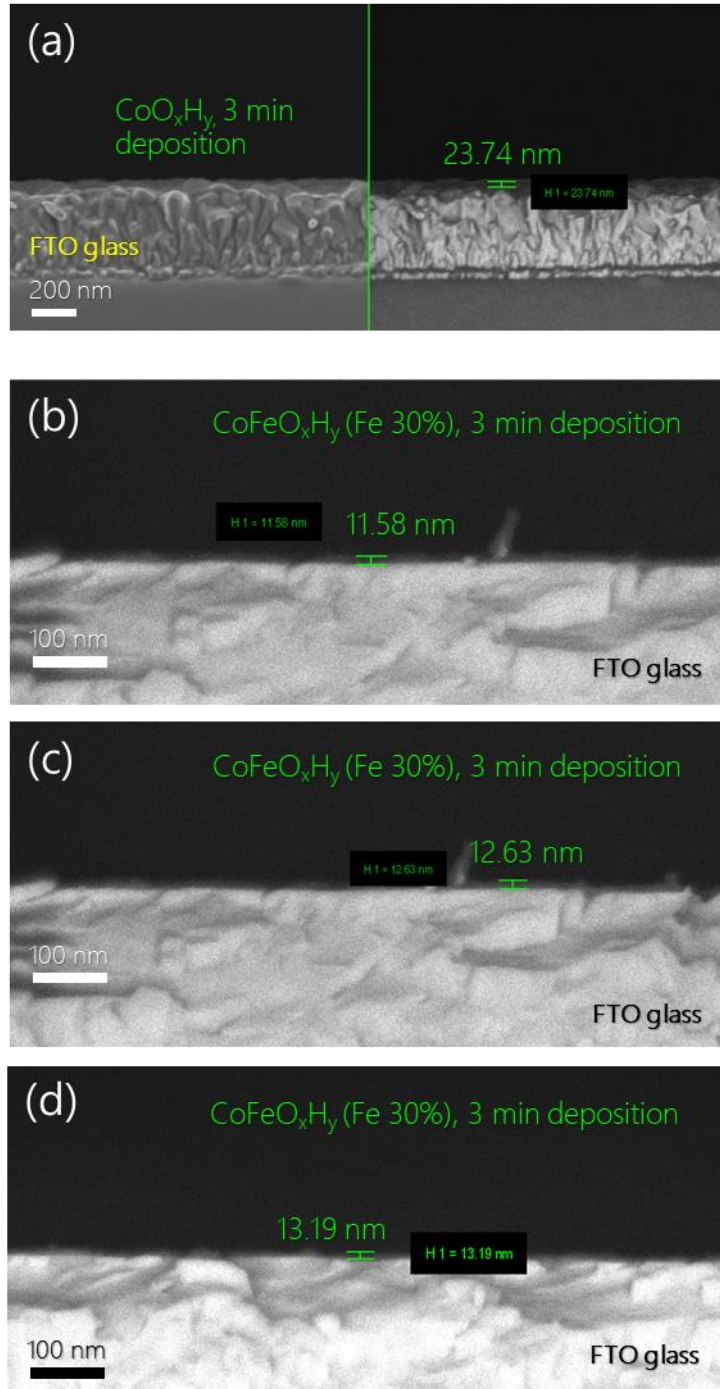


Figure S1. SEM images of CoO_xH_y and CoFeO_xH_y (Fe 30%) samples: Side view images of (a) CoO_xH_y and (b-d) CoFeO_xH_y films anodically deposited at 55.6 $\mu\text{A cm}^{-2}$ for 3 min. The different thickness between the two samples suggests that the deposition rate is dependent of electrolyte compositions. Hence, we applied different deposition times for the preparation of samples with different Fe contents.

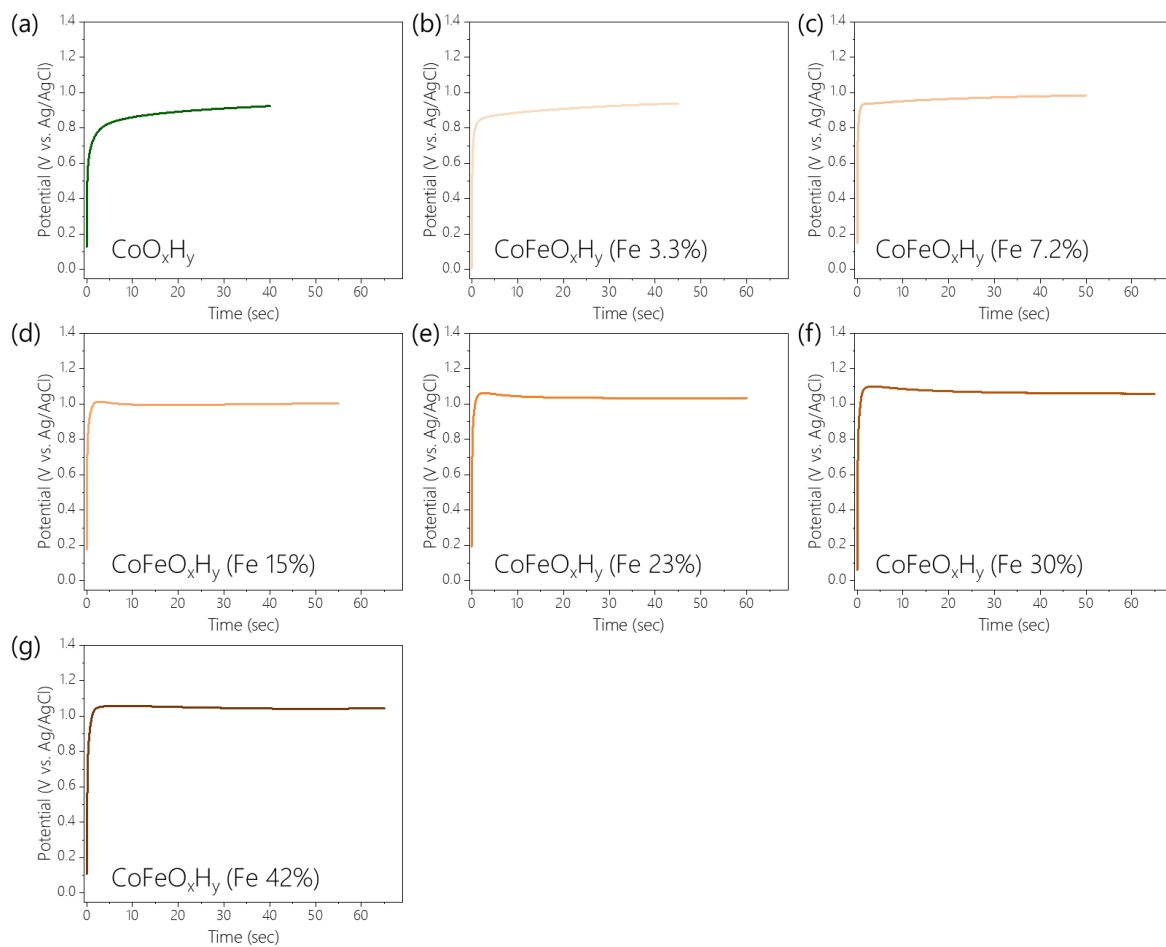


Figure S2. Potential profiles of the samples versus deposition time at a constant anodic current density of $55.6 \mu\text{A cm}^{-2}$.

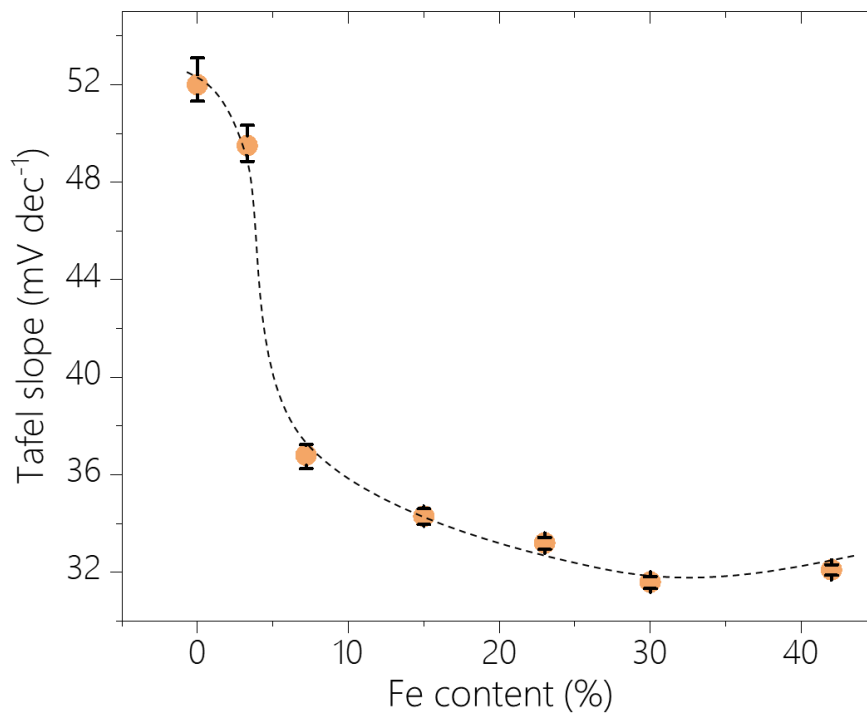


Figure S3. Comparison of Tafel slopes for the CoFeO_xH_y samples with different Fe contents.

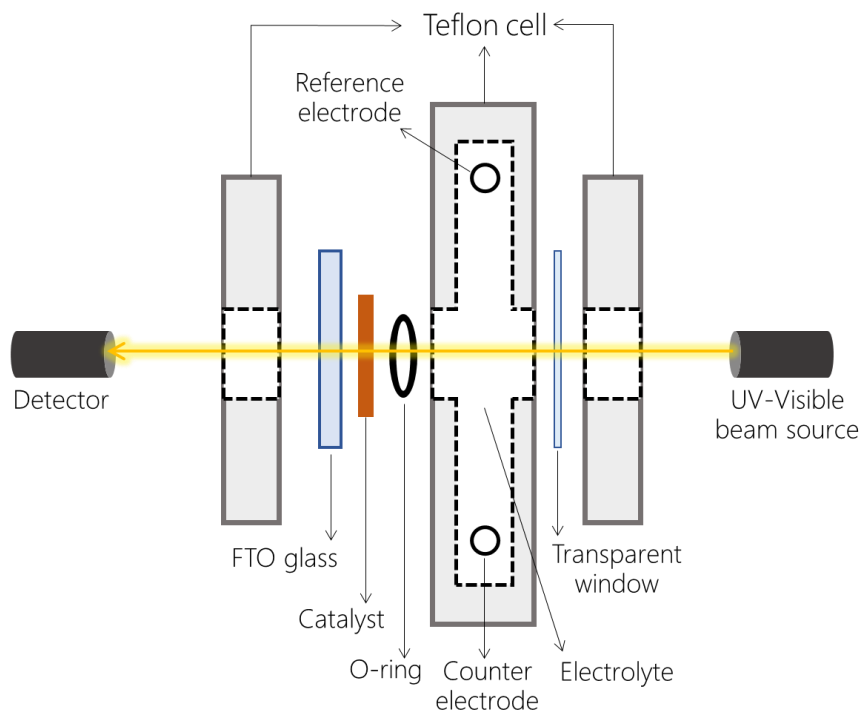


Figure S4. Scheme (top view) of a customized cell for the operando UV-Vis spectroscopy study.

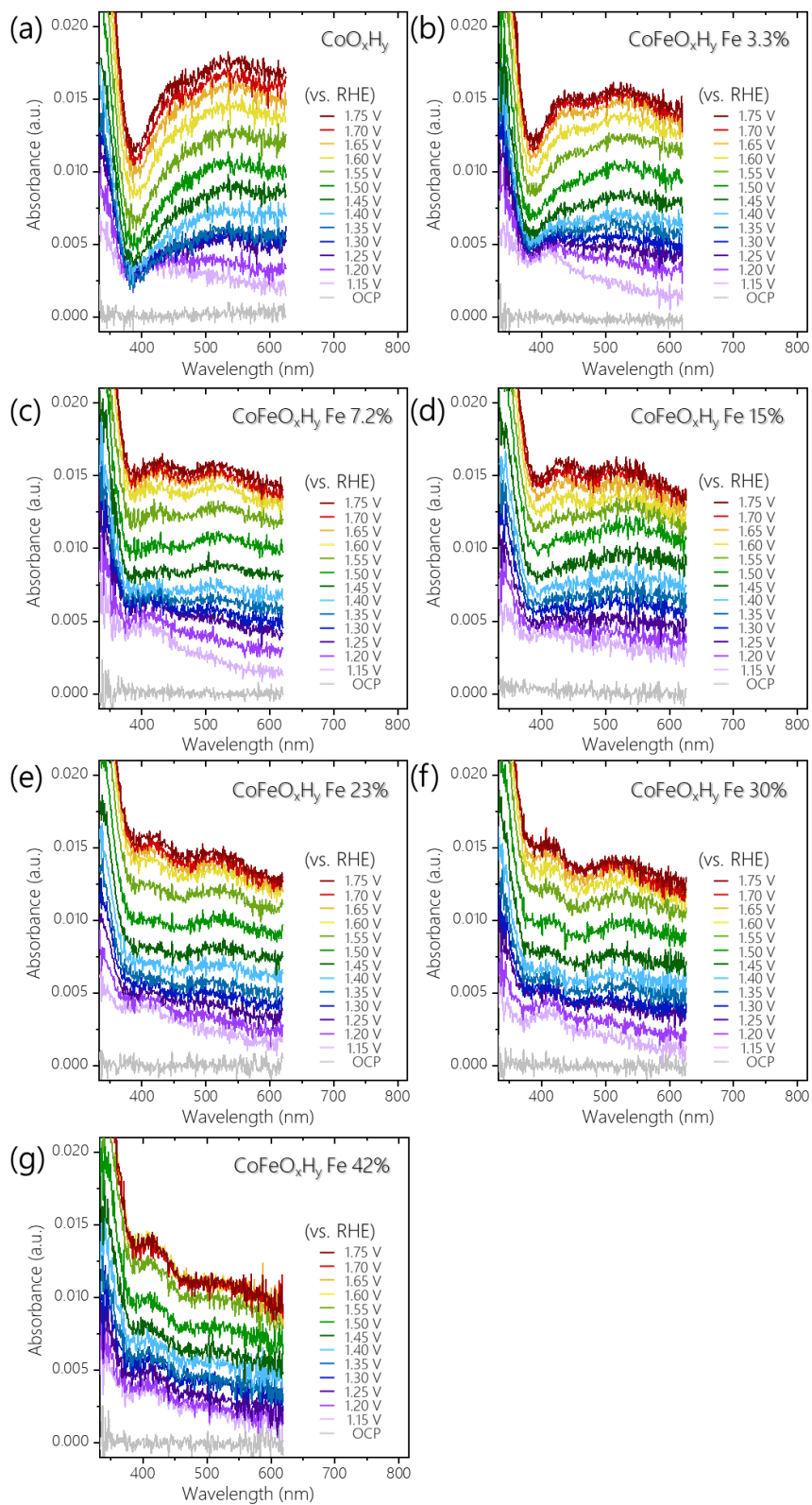


Figure S5. Operando UV-Vis spectra of CoO_xH_y and CoFeO_xH_y films (a-g). The spectra were obtained at each constant potential in 0.1 M Fe-free KOH from OCP to 1.75 V with an interval of 0.05 V.

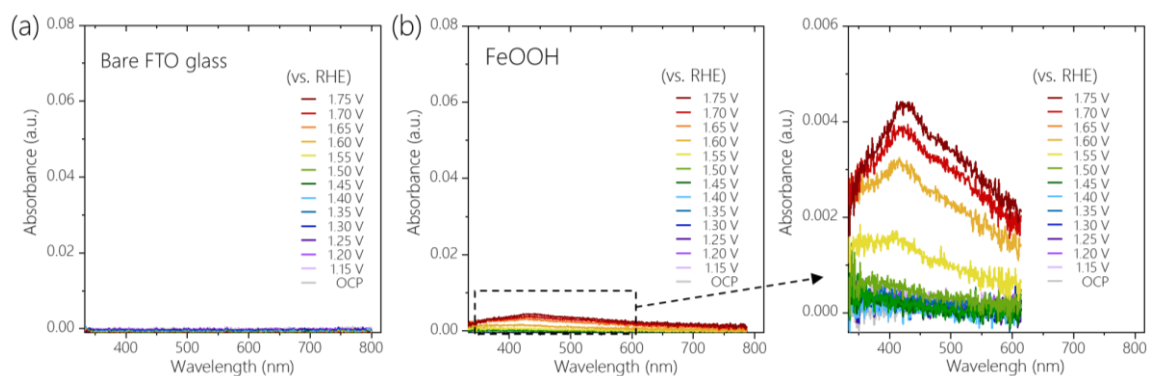


Figure S6. Operando UV-Vis spectra of (a) bare FTO glass and (b) FeOOH obtained at each constant potential in 0.1 M Fe-free KOH from OCP to 1.75 V with an interval of 0.05 V.

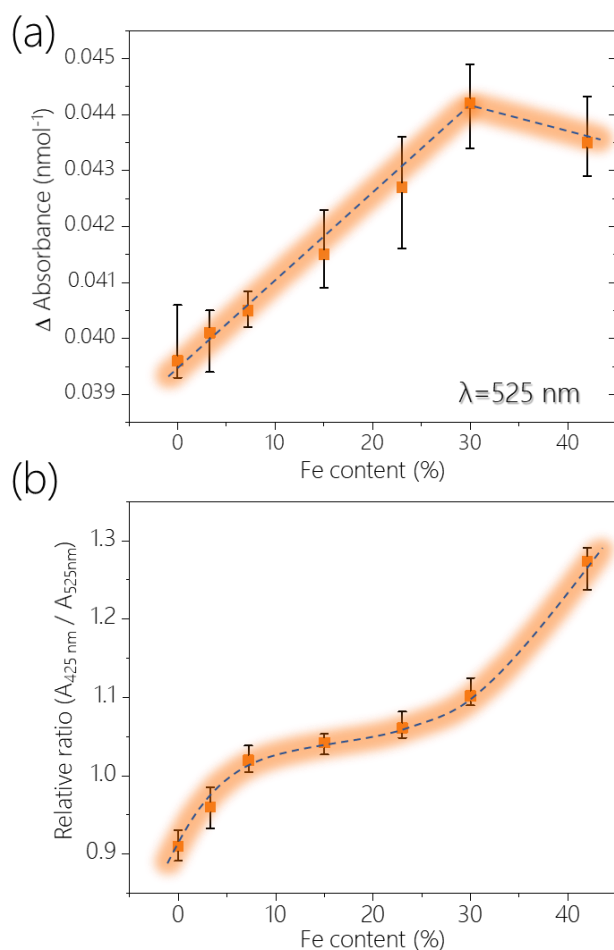


Figure S7. (a) Differential absorbance of the peak at 525 nm between OCP and 1.75 V for CoFeO_xH_y with different Fe content. (b) Relative intensity ratio of the peaks at 425 nm and 525 nm in CoFeO_xH_y samples with different Fe content.

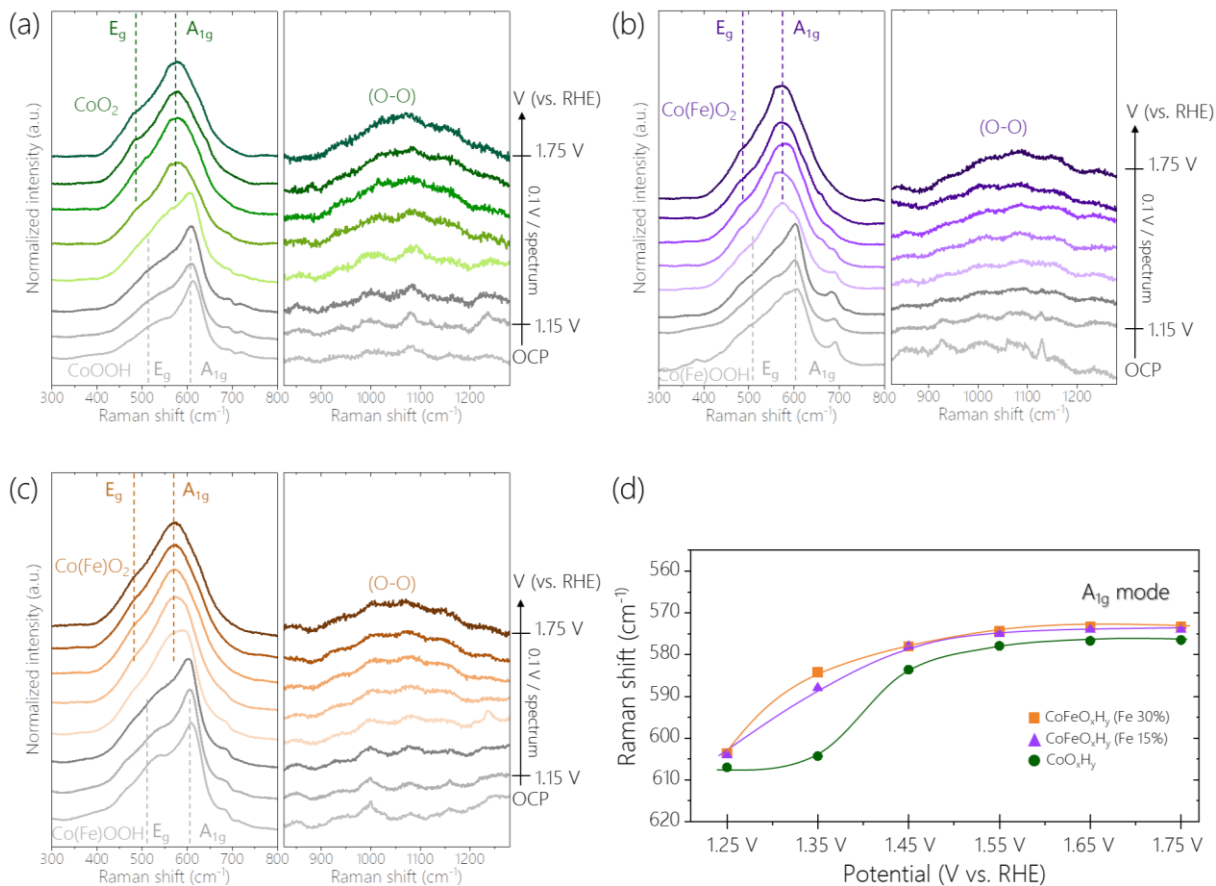


Figure S8. Operando Raman spectra of (a) CoO_xH_y and CoFeO_xH_y containing (b) 15% Fe and (c) 30% Fe at increasing applied potentials from OCP to 1.75 V (0.1 V per step) in 0.1 M Fe-free KOH solutions. (d) Comparison of potential dependent peak positions of the A_{1g} mode corresponding to Co–O stretching bond.

For all samples at OCP, two main peaks corresponding to E_g (at ca. 505 cm⁻¹) and A_{1g} (at ca. 605 cm⁻¹) vibrational modes of Co–O bonds in CoOOH were observed (Figure S8), consistent with a previous study.¹ With increasing applied potentials, these two peaks shifted to lower frequencies, indicating gradual oxidation of Co³⁺ to Co⁴⁺. The peaks stabilized at ca. 475 cm⁻¹ and ca. 575 cm⁻¹, corresponding to E_g and A_{1g} modes of Co(Fe)O₂ respectively. To probe Fe-dependent enhancement of Co oxidation to Co⁴⁺, we compared peak positions of the A_{1g} mode of Co–O for all three samples as function of potential (Figure S8d). The shift occurred at potentials in the order CoFeO_xH_y (30% Fe) < CoFeO_xH_y (15% Fe) < CoO_xH_y. This result shows Fe promotes the oxidation of Co³⁺ to Co⁴⁺.

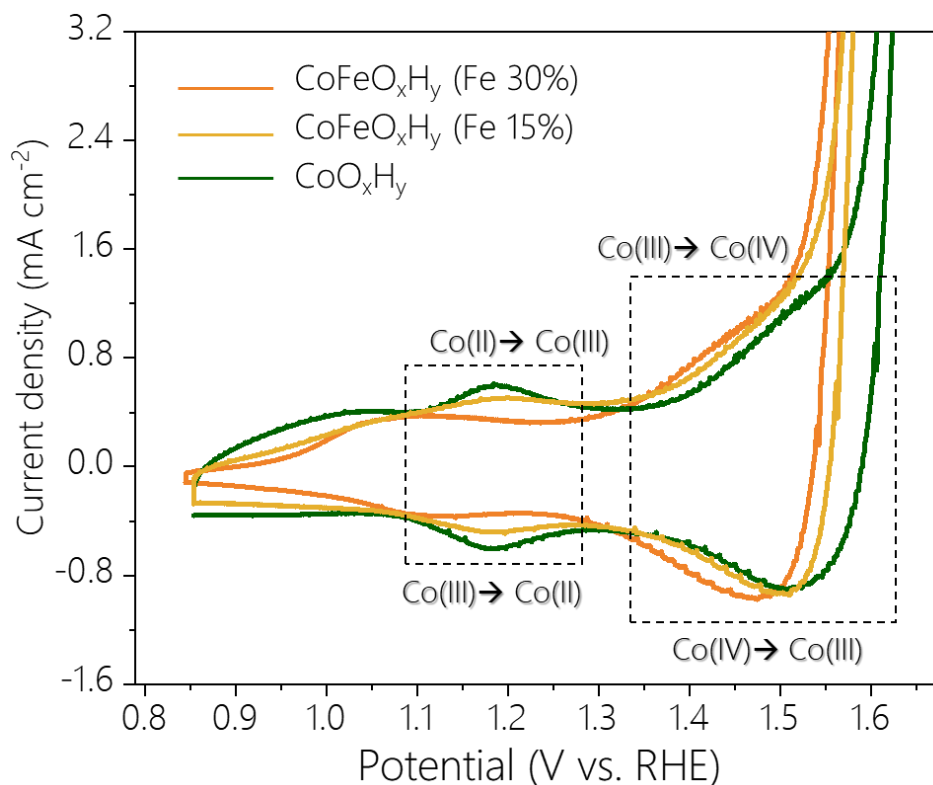


Figure S9. Cyclic voltammograms of CoFeO_xH_y samples containing 0%, 15% and 30% Fe obtained at a scan rate of 100 mV s⁻¹ in 0.1 M Fe-free KOH electrolyte.

At around 1.2 V, the pairs of redox events are attributed to the Co²⁺/Co³⁺ redox couple.¹⁻³ The second redox events in 1.4 V to 1.55 V are assigned to the Co³⁺/Co⁴⁺ redox couple.^{1, 2} The onset potentials for the oxidation to Co⁴⁺ depend on the Fe content. The more Fe is added, the earlier the Co³⁺ is oxidized.

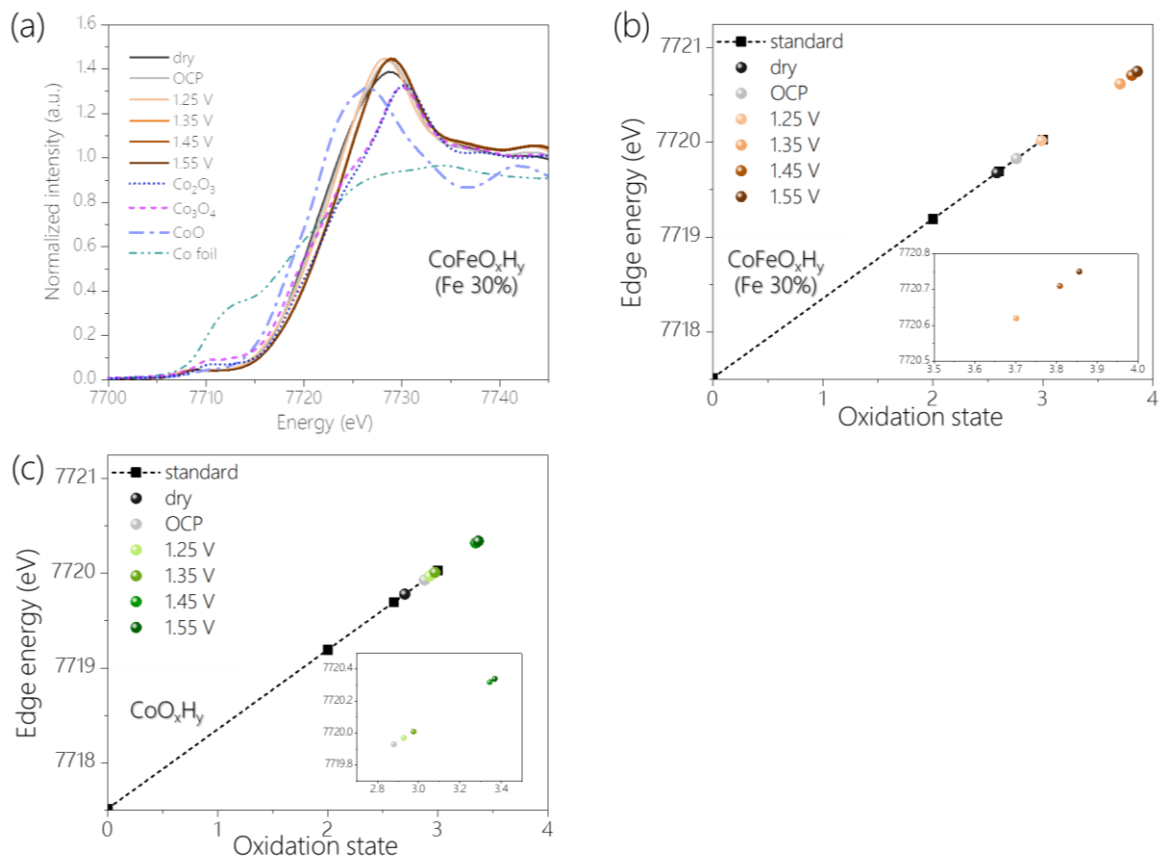


Figure S10. (a) XANES spectra of CoFeO_xH_y (30%Fe) for Co K-edge at various potentials; reference spectra include those of Co foil, CoO, Co_3O_4 , and Co_2O_3 . (b) The corresponding linear fit of Co oxidation state for CoFeO_xH_y . (c) Reproduced data of Co oxidation state for CoO_xH_y as reported earlier.¹

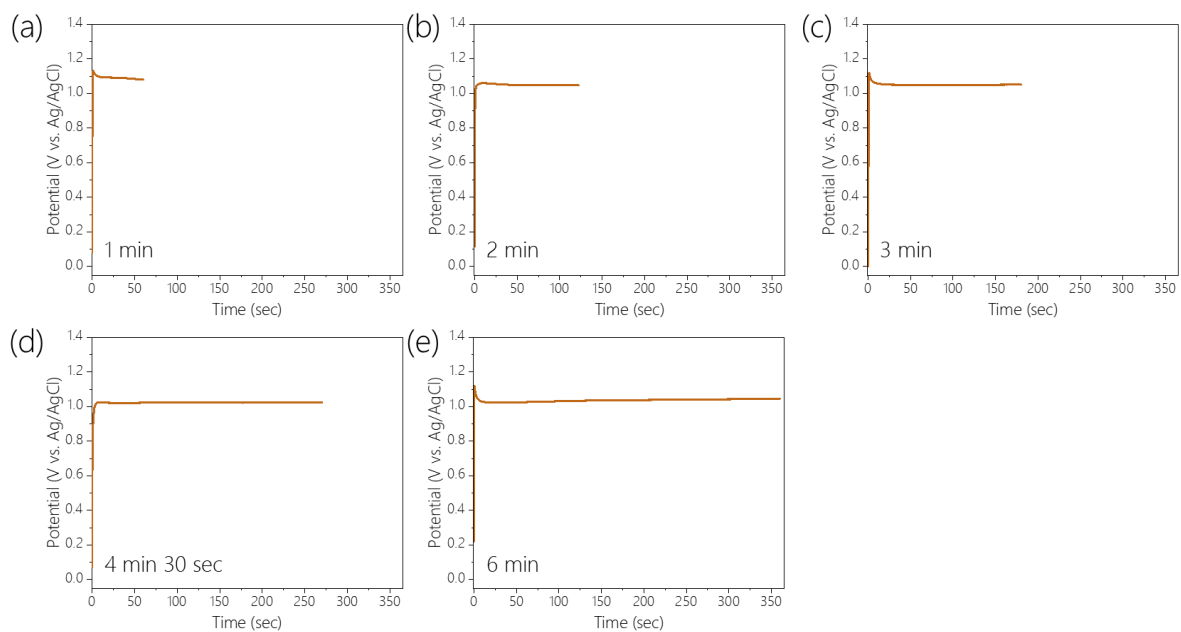


Figure S11. Potential profiles of the CoFeO_xH_y films (Fe 30%) at a constant anodic current density of 55.6 μA cm⁻².

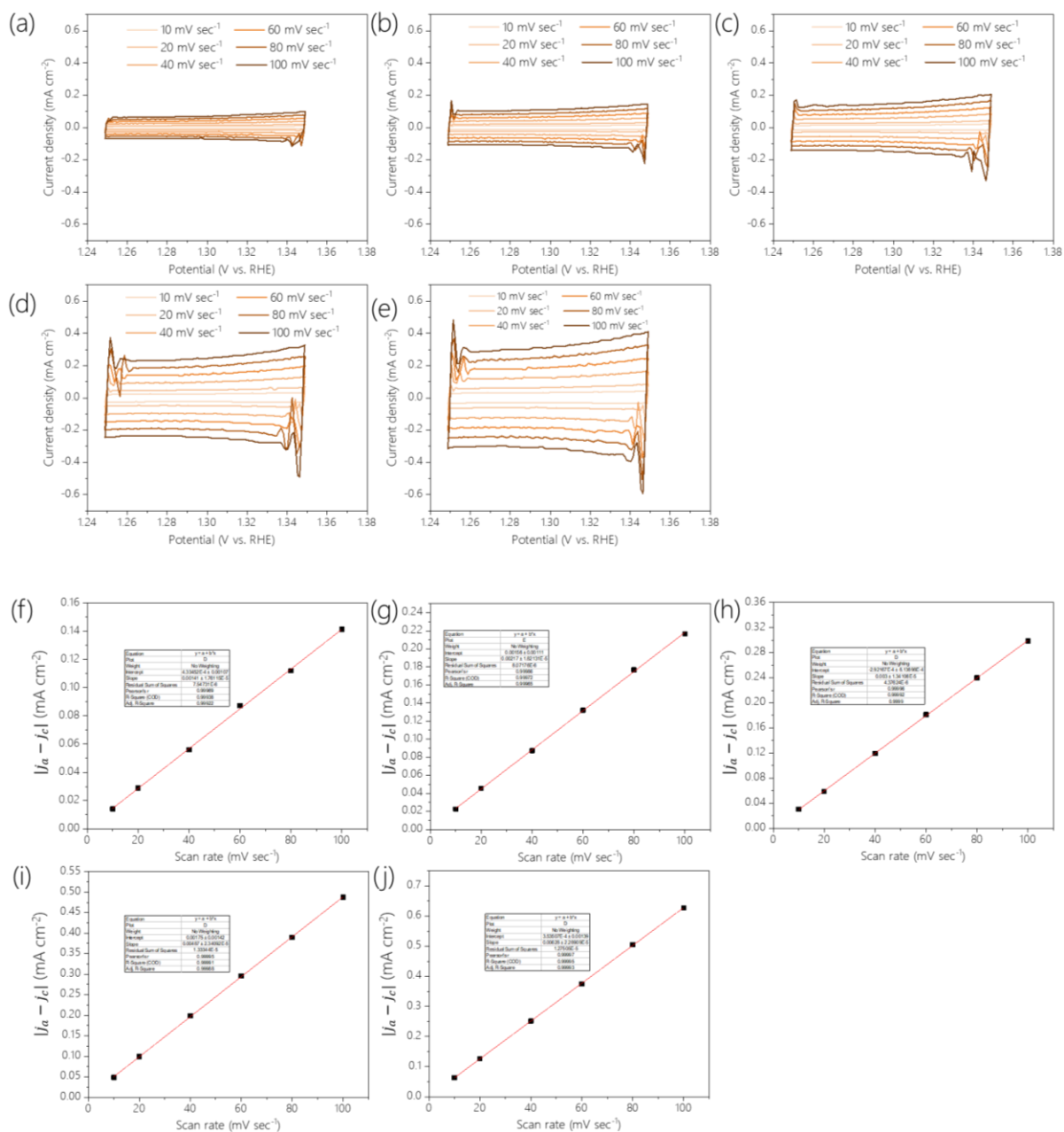


Figure S12. Cyclic voltammograms of the CoFeO_xH_y (Fe 30%) deposited for (a) 1 min, (b) 2 min, (c) 3 min, (d) 4 min 30 sec and (e) 6 min respectively, acquired in 0.1 M Fe-free KOH solutions at different scan rates (10, 20, 40, 60, 80, 100 mV sec^{-1}) for the determination of the C_{dl} . (f-j) Plots of the corresponding differences of the anodic and cathodic current densities, $\Delta J = |j_a - j_c|$, versus the scan rate (10, 20, 40, 60, 80, 100 mV sec^{-1}).

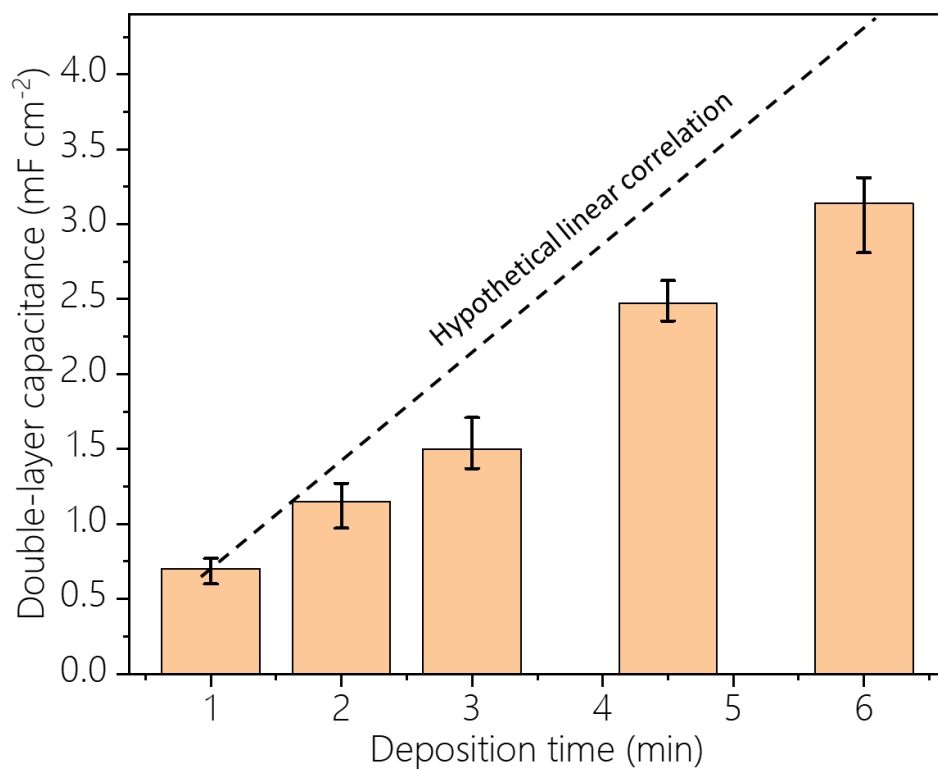


Figure S13. Comparison of double-layer capacitances (C_{dl}) for the CoFeO_xH_y (30%Fe) samples deposited at given deposition times. The C_{dl} gradually deviates from the linear correlation with increasing film thickness.

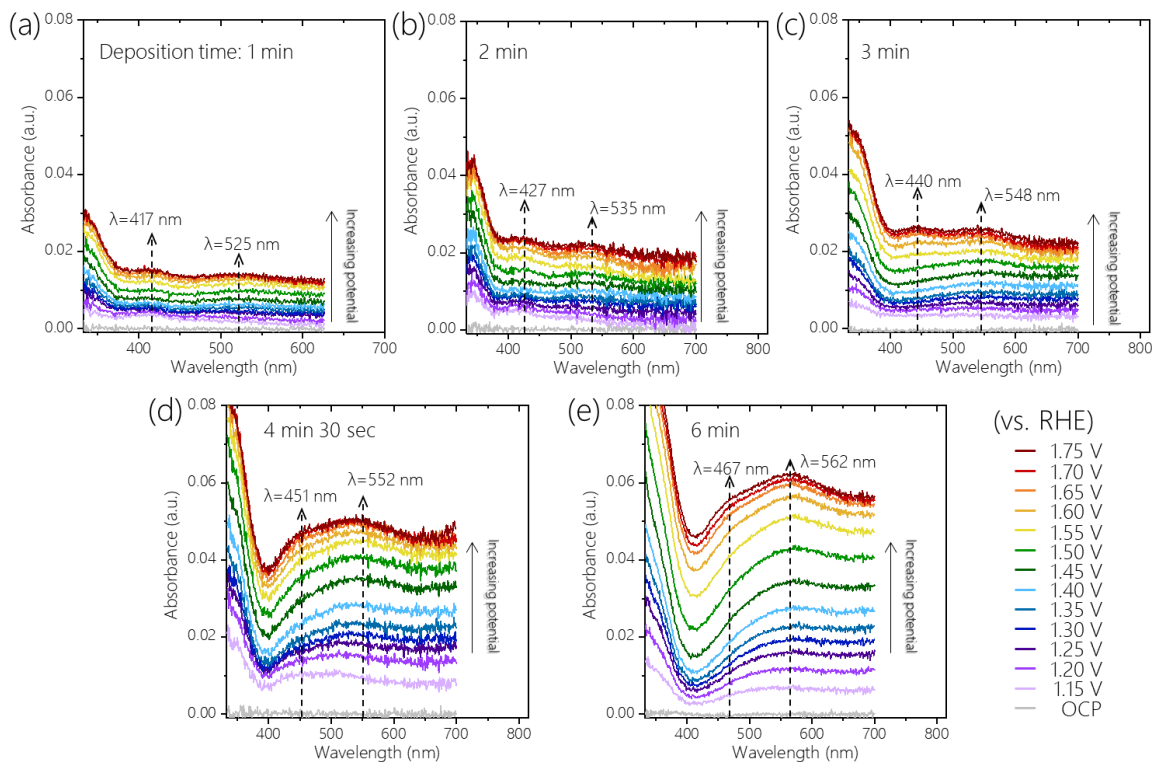


Figure S14. Operando UV-Vis spectra of the CoFeO_xH_y films (30%Fe) deposited for (a) 1 min, (b) 2 min, (c) 3 min, (d) 4 min 30 sec and (e) 6 min. The spectra were obtained at each constant potential in 0.1 M Fe-free KOH solutions from OCP to 1.75 V with an interval of 0.05 V.

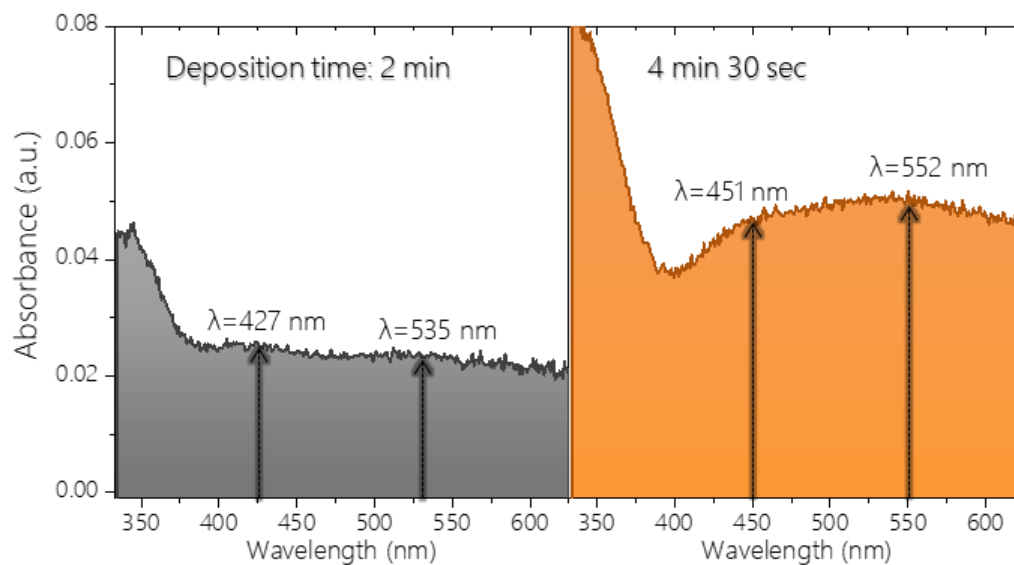


Figure S15. Operando UV-Vis spectra of CoFeO_xH_y (30% Fe) films prepared at various deposition durations such as (left) 2 min and (right) 4 min 30 sec at 1.75 V (vs. RHE).

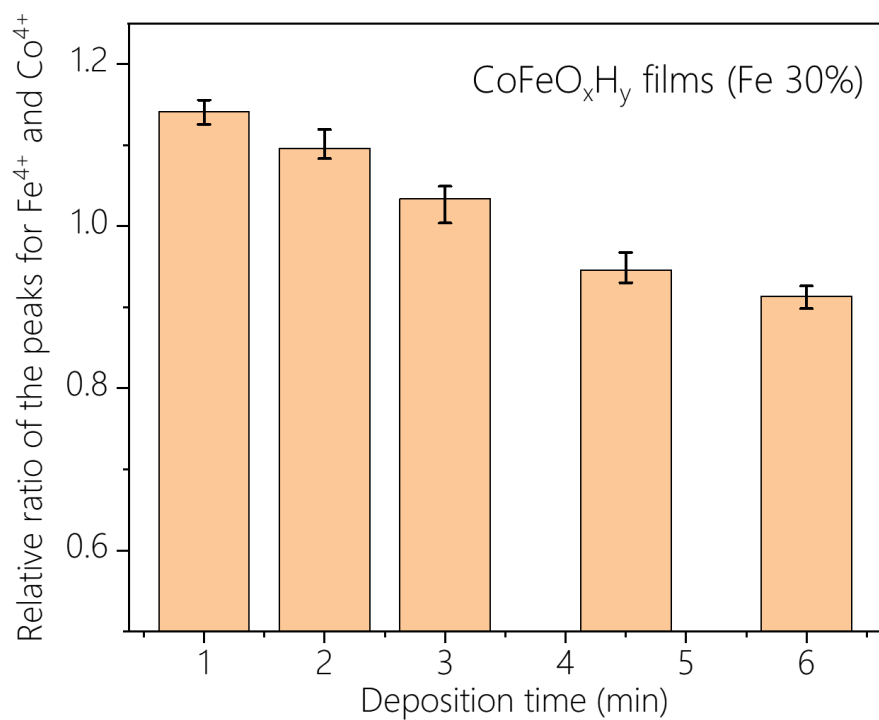


Figure S16. Comparison of relative ratio of the peak intensities associated with the Fe⁴⁺ and Co⁴⁺ for the CoFeO_xH_y (30%Fe) samples. The spectra were collected at 1.75 V in 0.1 M Fe-free KOH solutions.

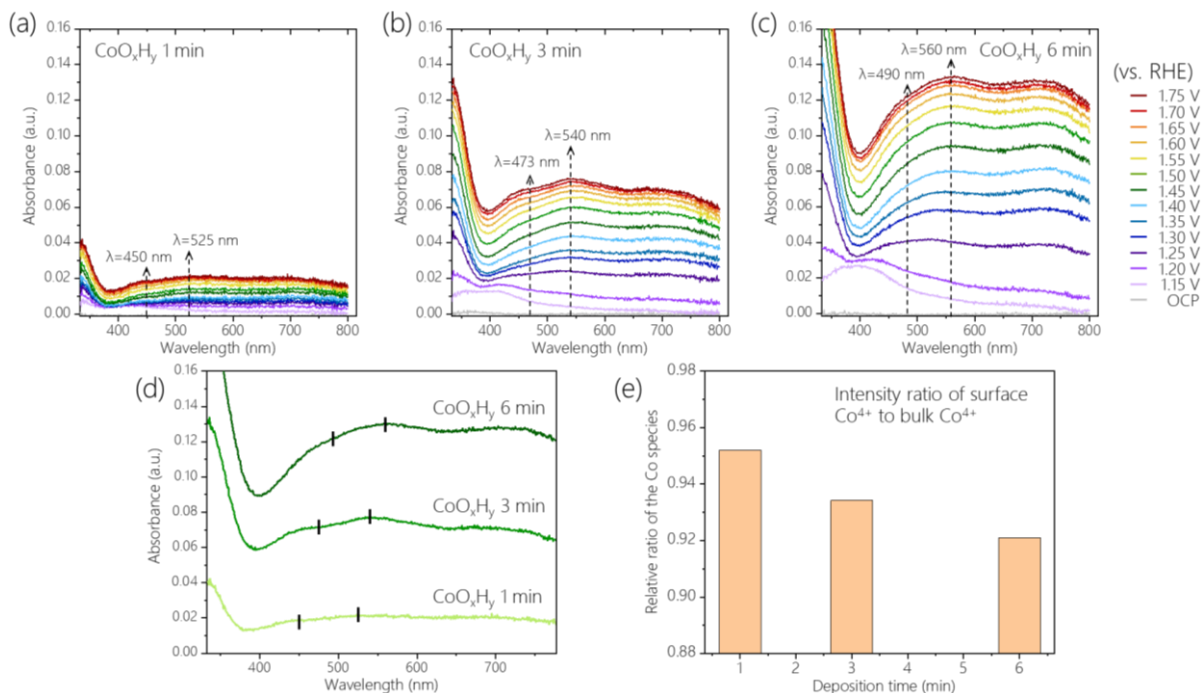


Figure S17. Operando UV-Vis spectra of the CoO_xH_y films deposited for (a) 1 min, (b) 3 min and (c) 6 min. (d) The representative spectra of the different CoO_xH_y films at 1.75 V. (e) Comparison of relative ratio of the peak intensities associated with the active Co species (450-490 nm) and Co^{4+} distributed in the entire bulk (525-560 nm) for CoO_xH_y samples with different thicknesses (deposition times). The spectra were collected at each constant potential in 0.1 M Fe-free KOH solutions from OCP to 1.75 V with an interval of 0.05 V.

For different CoO_xH_y films, two pronounced features were observed. The peaks assigned to high-valent Co species at the surface and Co^{4+} in the entire bulk shifted to higher wavelengths with increasing film thickness. The intensity ratio of the two Co species (e.g., $A_{450\text{nm}}/A_{525\text{nm}}$ for the 1 min-deposited sample) decreased upon increasing thickness. The result indicates that the proportion of high-valent Co species at lower wavelengths decreases as the film gets thicker, while the proportion of the Co^{4+} at higher wavelengths increases. This result is similar to the comparison of Fe^{4+} and Co^{4+} species in CoFeO_xH_y . Together, they support that the Co^{4+} species associated with the peak at higher wavelengths (i.e., 525 nm, 540 nm and 560 nm) is throughout the entire bulk.

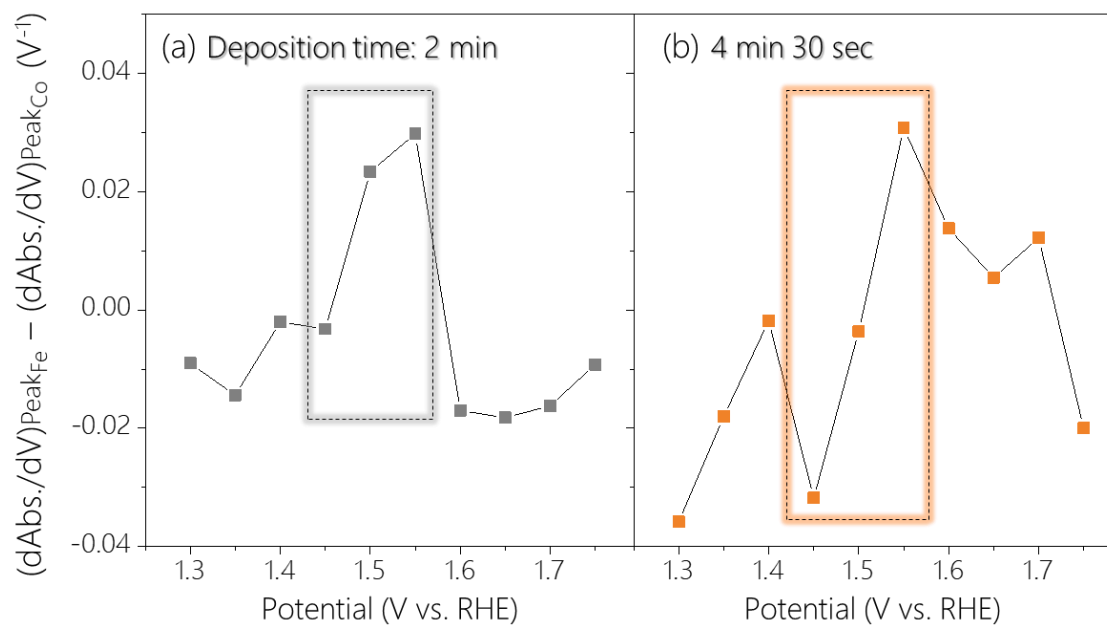


Figure S18. Difference in differential absorbance between the peaks of Fe⁴⁺ and Co⁴⁺ for CoFeO_xH_y samples (30%Fe) deposited for (a) 2 min and (b) 4 min 30 sec, respectively.

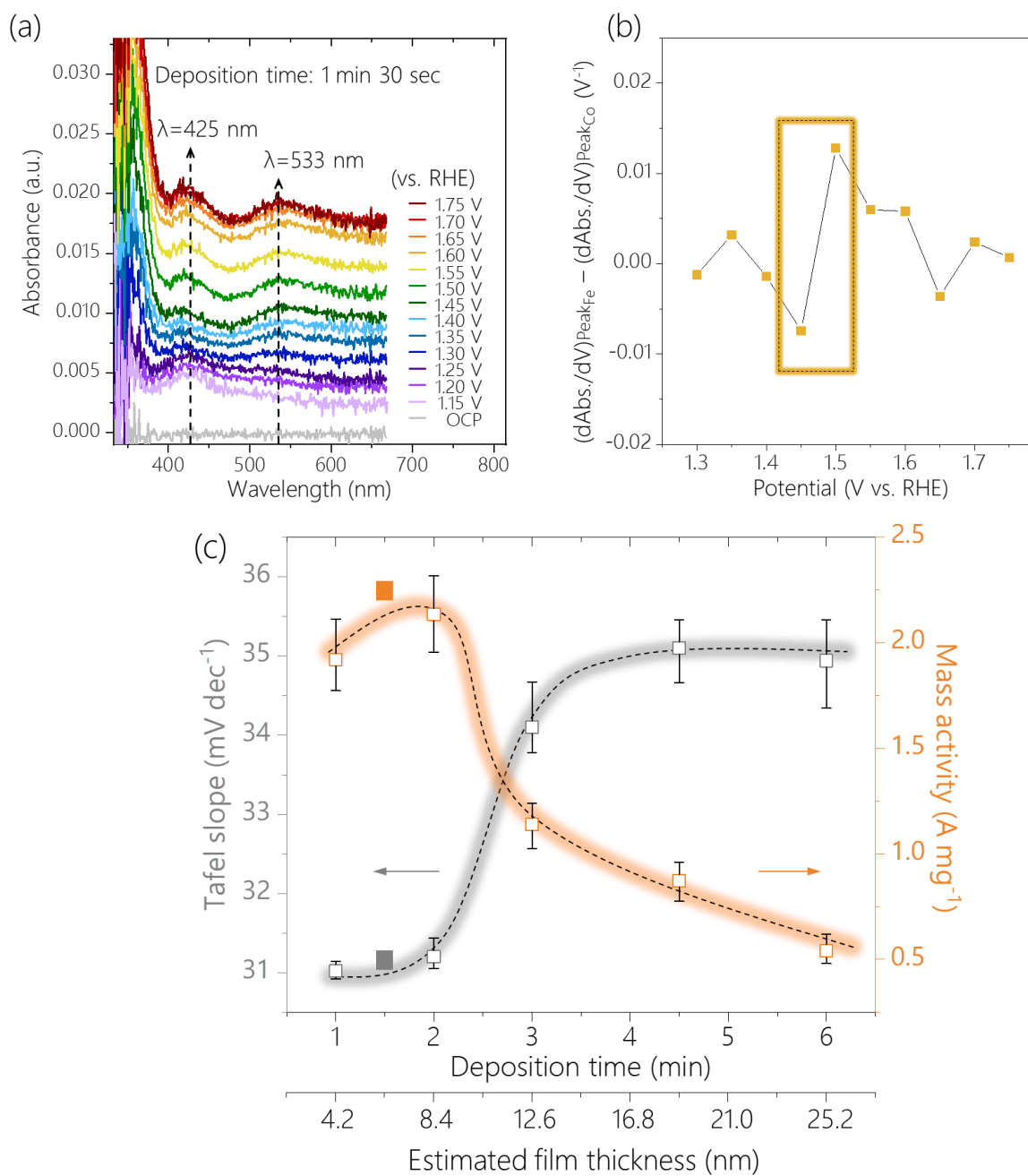


Figure S19. Experimental results obtained from CoFeO_xH_y (30%Fe) film deposited for 1 min 30 sec. (a) Operando UV-Vis spectra recorded from OCP to 1.75 V with 0.05 V per step. (b) Difference in differential absorbance between the peaks of Fe⁴⁺ and Co⁴⁺, derived from Figure S14a. (c) Comparison of Tafel slope and mass activity (at an overpotential of 340 mV) as function of deposition time and estimated film thickness, to which the data for the 1 min 30 sec deposited-sample are added.

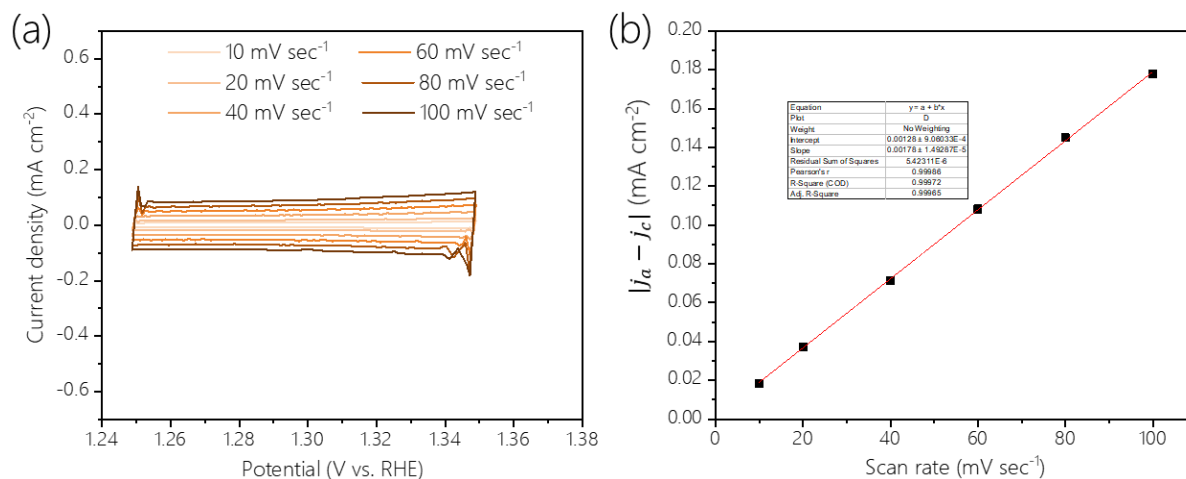
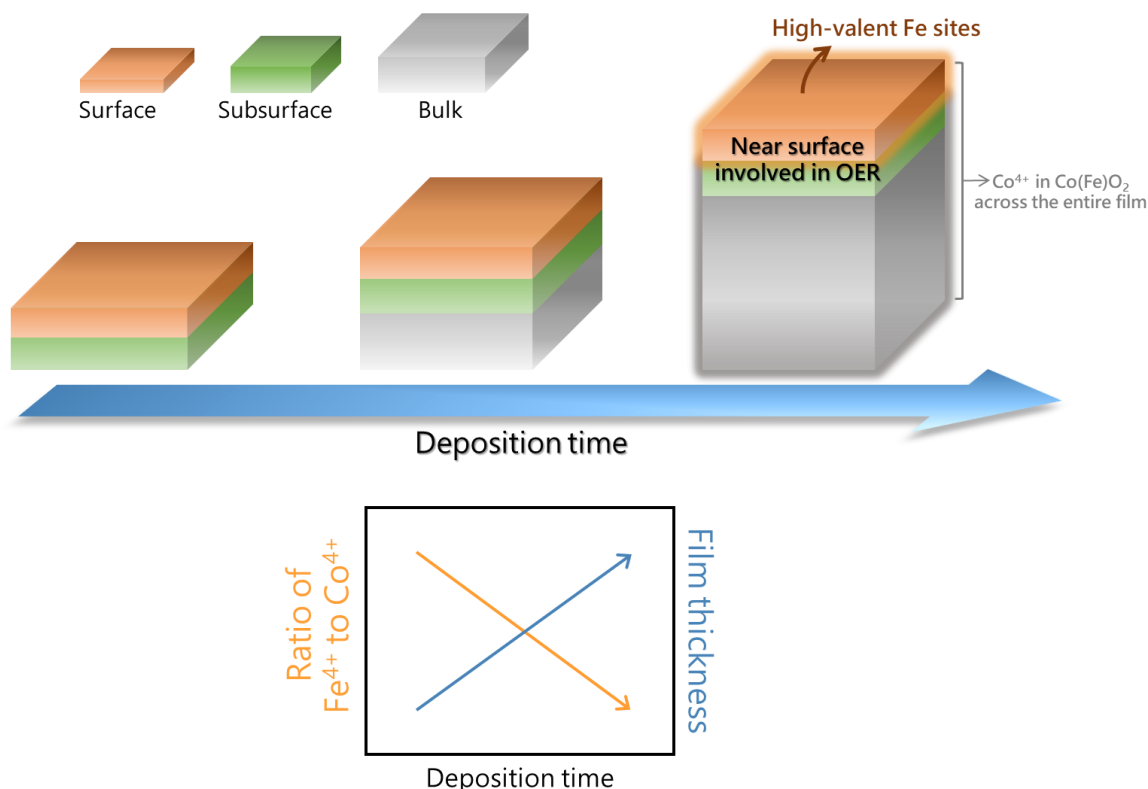


Figure S20. (a) Cyclic voltammograms of CoFeO_xH_y (30%Fe) deposited for 1 min 30 sec acquired in 0.1 M Fe-free KOH solutions at different scan rates (10, 20, 40, 60, 80, 100 mV sec⁻¹) for the determination of the C_{dl}. (b) A plot of the corresponding differences of the anodic and cathodic current densities, $\Delta j = |j_a - j_c|$, versus the scan rate (10, 20, 40, 60, 80, 100 mV sec⁻¹). The resulting C_{dl} was 0.89 mF cm⁻².

Appendix 1. Differentiating bulk and surface species in $\text{Co(Fe)O}_x\text{H}_y$ catalysts

We plotted $\log(\text{current density})$ versus normalized absorbance of the peaks at 450 nm for CoO_xH_y and 425 nm for CoFeO_xH_y (Fe 30%) (Figure 3). They are assumed to represent the accumulation of high-valent, catalytically active Co (e.g., $\text{Co}^{4+}\text{-O}\cdot\text{-Co}^{4+}$) and Fe (Fe^{4+}) species respectively. The concentration of $\text{Co}^{4+}\text{-O}\cdot\text{-Co}^{4+}$ and Fe^{4+} scales with the corresponding $\log(\text{current density})$, suggesting that they are active species for CoO_xH_y and CoFeO_xH_y , respectively. In contrast, the change in absorbance at 525 nm (assigned to Co^{4+} in the bulk) for both samples does not scale with the OER activity, suggesting that this species is not the active species. At Fe contents higher than 3.3%, the peak for $\text{Co}^{4+}\text{-O}\cdot\text{-Co}^{4+}$ (450 nm) is no longer observed during OER (Figures 2c and S5). The results indicate a change of active sites from CoO_xH_y to CoFeO_xH_y .



Scheme S1. Testing the hypothesis that Fe^{4+} sites are at the surface by studying films of different thickness

The ratio of surface sites versus bulk sites will decrease with increasing film thickness (Scheme S1). If the Fe^{4+} active sites in CoFeO_xH_y are at the surface, and the Co^{4+} sites are in the bulk, then the intensity of the peaks corresponding to Fe^{4+} (425 nm) and Co^{4+} (525 nm) will decrease with increasing film thickness. Concomitantly the

metal mass-based OER activity will decrease. If both sites are in the bulk, or both sites are on the surface, then the ratio should be constant. If Fe^{4+} active sites are in the bulk and Co^{4+} sites are on the surface, then the ratio would increase with increasing film thickness.

We found that with increasing in film thickness, the ratio of the absorption intensities for the Fe^{4+} and Co^{4+} (e.g., $A_{417\text{nm}}/A_{525\text{nm}}$ for the 1 min-deposited sample) at 1.75 V gradually decreased (Figure S16) when the thickness was increased. The metal mass-based OER activity also decreased with increasing film thickness (Figure 4c). These results can only be explained if we consider the Fe^{4+} active sites in CoFeO_xH_y are at the surface, and the Co^{4+} sites are in the bulk. The result is consistent with previous studies that showed that OER catalysis was often limited to near surface sites.⁴⁻⁸

References

1. A. Moysiadou, S. Lee, C.-S. Hsu, H. M. Chen and X. Hu, *J. Am. Chem. Soc.*, 2020, **142**, 11901-11914.
2. J. A. Koza, Z. He, A. S. Miller and J. A. Switzer, *Chem. Mater.*, 2012, **24**, 3567-3573.
3. M. S. Burke, M. G. Kast, L. Trotochaud, A. M. Smith and S. W. Boettcher, *J. Am. Chem. Soc.*, 2015, **137**, 3638-3648.
4. S. Corby, M.-G. Tecedor, S. Tengeler, C. Steinert, B. Moss, C. A. Mesa, H. F. Heiba, A. A. Wilson, B. Kaiser, W. Jaegermann, L. Francàs, S. Gimenez and J. R. Durrant, *Sustain. Energy Fuels*, 2020, **4**, 5024-5030.
5. H. N. Nong, L. J. Falling, A. Bergmann, M. Klingenhof, H. P. Tran, C. Spöri, R. Mom, J. Timoshenko, G. Zichittella, A. Knop-Gericke, S. Piccinin, J. Pérez-Ramírez, B. R. Cuenya, R. Schlögl, P. Strasser, D. Teschner and T. E. Jones, *Nature*, 2020, **587**, 408-413.
6. C. Roy, B. Sebok, S. B. Scott, E. M. Fiordaliso, J. E. Sørensen, A. Bodin, D. B. Trimarco, C. D. Damsgaard, P. C. K. Vesborg, O. Hansen, I. E. L. Stephens, J. Kibsgaard and I. Chorkendorff, *Nat. Catal.*, 2018, **1**, 820-829.
7. B. S. Yeo and A. T. Bell, *J. Am. Chem. Soc.*, 2011, **133**, 5587-5593.
8. C. Baeumer, J. Li, Q. Lu, A. Y.-L. Liang, L. Jin, H. P. Martins, T. Duchoň, M. Glöß, S. M. Gericke, M. A. Wohlgemuth, M. Giesen, E. E. Penn, R. Dittmann, F. Gunkel, R. Waser, M. Bajdich, S. Nemsák, J. T. Mefford and W. C. Chueh, *Nat. Mater.*, 2021, **20**, 674-682.